INNSPUB

Journal of Biodiversity and Environmental Sciences (JBES)
ISSN: 2220-6663 (Print) 2222-3045 (Online)
Vol. 22, No. 5, p. 134-142, 2023
http://www.innspub.net

RESEARCH PAPER OPEN ACCESS

# Studies on synthesis, characterization and photocatalytic activity of activated charcoal doped chitosan (AC-CS)

**P. Bhuvaneswari[1], T. Shanmugavadivu[1], G. Sabeena[2], G. Annadurai[2], E. Sindhuja[*1]**

[1]*Department of Chemistry, Sri Paramakalyani College, Manonmaniam Sundaranar University, Alwarkurichi, Tamil Nadu, India*

[2]*Sri Paramakalyani Centre of Excellence in Environmental Sciences, Manonmaniam Sundaranar University, Alwarkurichi, Tamil Nadu, India*

Article published on May 18, 2023

**Key words:** Activated carbon, Chitosan, FTIR, SEM, TGA, Malachite green dye, Photocatalytic activity

**Abstract**

In this study, activated charcoal doped chitosan (AC-CS) was effectively synthesized, and the material was then examined using XRD, FTIR, SEM-EDX, and UV. Results demonstrate that activated charcoal doped chitosan (AC-CS) has a characteristic binding crystalline structure with an average size of 50nm and aggregates of minute fibres in diverse sizes and shapes. Chitosan doped with activated charcoal exhibits UV absorption bands with maximal wavelengths at 308nm. To evaluate the photocatalytic performance of the activated charcoal doped chitosan (AC-CS), Malachite Green dye degradation was utilized. Chitosan that has been doped with activated charcoal (AC-CS) was applied to boost the photocatalytic activity towards the Malachite Green dye. The performance of the photocatalytic reaction was significantly improved by supporting the active charcoal doped chitosan (AC-CS).

***Corresponding Author:** E. Sindhuja ✉ sindhujaelangovan@gmail.com

## Introduction

According to Aragunde *et al.* (2018), chitosan (CS) is a linear heteropolysaccharide made up of n-acetylglucosamine and 1,4-glucosamine, which is produced when chitin is deacetylated. According to studies looking at chitosan as a natural biopolymer, it has increased biocompatibility and biodegradability and reduced immunogenicity (Annu *et al.*, 2020; Manzoor *et al.*, 2019; Samadian *et al.*, 2020; Sumayya *et al.*, 2017). Chitosan also has an alkaline pH and the capacity to degrade into innocuous substances that may be eliminated from the body (Vichare *et al.*, 2020). As a secure drug delivery method, chitosan has been widely used in the pharmaceutical industry (Fu *et al.*, 2017, Onishi *et al.*, 2020). Additionally, it demonstrates targeted anticancer (Tan *et al.*, 2018), antiviral, and antibacterial activities against a variety of bacteria and fungi (Costa *et al.*, 2012, Tan *et al.*, 2018).

Although the integration of polymeric matrices with nanofillers alters the mechanical strength, dye adsorption, and dye degradation properties of chitosan (Salari *et al.*, 2018, Sun *et al.*, 2020), this form of conjugated (chitosan doped inorganic materials) is attracting recognition (Tang *et al.*, 2012; Bhattacharyya *et al.*,2012; Sajid *et al.*, 2015). Due to its high efficacy, straightforward setup, simple operation, low energy requirement, and high oxidation capability, photocatalysis, a cutting-edge technique, has been used for the photodegradation of numerous organic contaminants. Scientists have focused a lot of attention in recent years on semiconductor photocatalysts as a means of resolving problems with the environment (Ullah *et al.*, 2008; Pouretedal *et al.*, 2009).

Heterogeneous photocatalysis has been regarded as a practical alternative method for water remediation among diverse physical, chemical, and biological techniques (He *et al.*, 2011). The advantages of photocatalytic technology over conventional ones in wastewater treatment are fast oxidation, high efficiency, no creation of polycyclic products, and low-level combustion of contaminants.

The most popular applications for malachite green (MG) include dyeing cotton, silk, paper, and leather as well as producing paints and printing inks. The aquatic life will be harmed, and the liver, gills, kidney, gut, and gonads will suffer.

This is because solutions containing MG should not be discharged into receiving streams (Onishi *et al.*, 2020; Maldiney *et al.*, 2014). A very effective way to overcome these limitations and enhance the physiochemical Chemical modification by cross-linking reaction utilising activated charcoal (AC) is one of the chitosan biopolymer's features.

Additionally, by using Activated Charcoal as a material with numerous functions/properties that eventually biodegrade to harmless products in the presence of water, it is possible to prevent widespread consumption, leakage, and buildup of chitosan doped activated charcoal in the environment (Jurki *et al.*, 2013). Although it has significant technological constraints, such as a high cost and a challenging recovery process, activated charcoal is also frequently employed in the treatment of water (Jung *et al.*, 2016a, b; Hassan *et al.*, 2017; Afzal *et al.*, 2018).

In this study, the objective was to create chitosan-doped activated charcoal using a straightforward, economical process that would enable large-scale preparation of the material. The substance was completely characterised before being used to decompose Malachite green dye in aqueous solutions.

## Materials and methods

The chemicals employed in this study consisted of analytical-grade materials that came through Merck in India. They have not been further purified and were employed straight in the source.

Along with activated charcoal, acetic acid as well as ethanol, Sigma-Aldrich offered chitosan which had gone through 90% deacetylation as a starting material. All preliminary procedures were finished using distilled water. Prior to further filtration, all analytical-grade chemicals and reagents were used.

*Preparation of Activated Charcoal doped chitosan (AC-CS)*

Activated Charcoal doped chitosan (AC-CS) was produced in a 2:1 ratio. First, 2g of raw chitosan and 1g of activated charcoal were mixed with 100ml of distilled water. After then, the mixture was shaking vigorously for two days. This mixture was applied to petriplates and dried thoroughly. Dried petriplates were then taken and soaked in sodium hydroxide solution within 30 minutes. Particle was collected in sheet form and washed with tap water twice or three times before being dried in a hot air oven for 24 hours at $60^0$ C and then calcined for four hours at $600^0$ C. Activated charcoal doped chitosan (AC-CS) sheets were then produced. Chitosan doped with activated charcoal (AC-CS) was gathered. (Nguyen *et al*., 2020).

*Application of manufactured activated charcoal doped chitosan (AC-CS) Photodegradation process*

The photocatalytic activity of activated charcoal doped chitosan (AC-CS) is assessed using the photocatalytic degradation of Malachite Green (MG) as a reaction probe in a beaker with stirring. 100 ml of solution Malachite Green (MG) from Scheme 1 was introduced to the reactors along with the required catalyst in order to conduct photocatalytic tests.

The solution was thoroughly mixed for 10 minutes in complete darkness before being exposed to radiation in order to achieve the process of adsorption equilibration of the framework. Following UV lamp irradiations, testing samples were collected at various time intervals, filtered, and then added to a quartz cell. A UV spectrophotometer set at = 540nm was used to measure the Malachite Green (MG) content at various times. All photocatalytic activities were carried out at room temperature. The photodegradation efficiency was calculated using the following equation:

$$\text{Photodegradation efficiency (\%)} = \frac{Co - Ce}{Co} \times 100$$

Where Ce is the dye's ultimate concentration following UV exposure, and Co is the dye's initial concentration (Owda *et al*., 2021).

*Characterization*

The molecular structure of the created hybrids was investigated using a Nicolet Magma 550 series II, made by Midac in the USA, at wavelengths between 4000 and 400cm-1. Dry film was pulverised with KBr powder and then smashed into discs for FTIR examination. To assess the physical characteristics of the samples, a JEOL (Japan) JSM-T300 scanning electron microscope with EDX (SEM-EDX) was employed. The sample was coated with gold using a JEOL JFC-110E ion sputter. Using a Bruker D8 Advance diffractometer with Cu K radiation (k = 1.540 A°) at 40 kV and 40 mA, XRD patterns were recorded. Scans were carried out with a detector step size of 0.02° and an angular range of 2 =10-80°. The bioreduction of metal particles in the structure was discovered using a UV-Vis spectrophotometer, with a spectrum from 200 to 800nm for each example taken against cleansed water as clear. An ultrasound treatment probe has previously been used to homogenise the mixture for five minutes.

**Result and discussion**

*X-Ray Diffraction Spectroscopy*

Fig 1 displays the XRD patterns of Activated Charcoal doped chitosan (AC-CS). The three main peaks are located at scattering angles (2) of 26.3°, 42.8°, and 79.6°, respectively. These depict the chitosan that has been polydispersed and formed into Activated Charcoal Doped Chitosan (AC-CS). The recorded literature and accepted references (Abdel *et al*., 2018; Bhadra *et al*., 2011; Li *et al*., 2010) fit the measured diffraction reflections well. There were no other diffraction peaks indicating any contaminants. According to the Debye-Scherer formula, the crystal size of activated charcoal doped chitosan (AC-CS) was determined through the widening of peak patterns of diffraction (Liu *et al*., 2019)

$$D = K\lambda/\beta \cos\theta$$

while D is the size of the crystal, k is constant (0.94), X-ray wavelength is represented by = 0.154nm, is the full width at half maximum of the dispersion peaks (FWHM) in radians, and is the Bragg's angle. Because the Activated Charcoal doped chitosan (AC-CS) diffraction peak displays a rather significant intensity and isn't

overlapping with other peaks, its crystal size was assessed. Chitosan that has been doped with activated charcoal often has crystals that are 50nm in size.

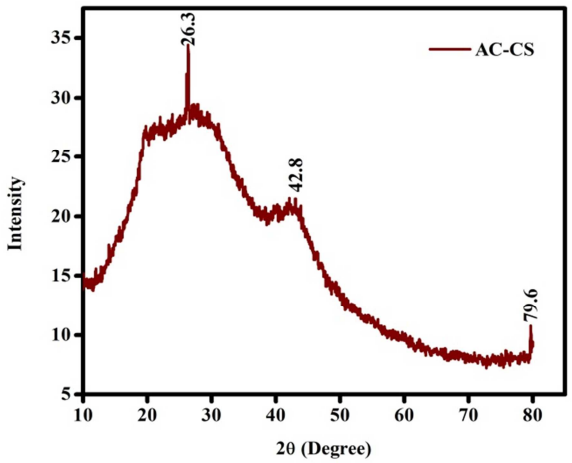


**Fig. 1.** The XRD graph of Activated Charcoal doped chitosan (AC-CS).

*Fourier Transform Infrared (FT-IR) Spectroscopy*

Fig 2 demonstrations the FTIR bands of Activated Charcoal doped chitosan (AC-CS), the peak at 2256cm−1corresponds toward the O-H extending vibration and the AC-CS outstanding to C-N axial alteration might be accountable aimed at the highest peak at 1560cm−1; the wide-ranging peak on 536cm−1 is outstanding toward the -OH/-NH2 stretching vibration; the peaks at 641 besides 452cm−1 remain credited toward the C-H stretching vibration; the peak at 413cm−1 resembles in the direction of the amino group bending vibrations; the peak at 401cm−1 might be outstanding on the way distortion of amide II; (Wang *et al.*, 2019; Lijun You *et al.*, 2018; Hasmath Farzana *et al.*, 2015; Huang *et al.*, 2017; Zabihi *et al.*, 2019).

These peaks demonstrated that chemical interactions, such as the creation of hydrogen bonds between the oxygen groups of the AC and the functional groups of the chitosan, were responsible for the effective grafting of the AC with chitosan (Sharififard *et al.*, 2018). Activated Charcoal is well-mixed and facilitates efficient dye removal by the Malachite Green dye Photodegradation process due to the presence of amide, amine, and hydroxyl functional groups. (Owda *et al.*, 2021).

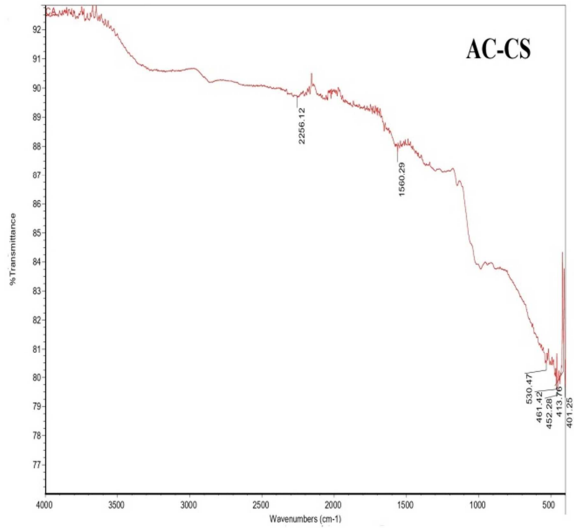


**Fig. 2.** The FTIR graph of Activated Charcoal doped chitosan (AC-CS).

*Scanning Electron Microscopy-EDX*

Whenever seen through SEM images, activated charcoal doped chitosan (AC-CS) displays a rough and uneven surface. Due to the abundance of pores and tunnels on materials like activated charcoal doped chitosan (AC-CS) as shown fig. 3.

This may suggest a high specific surface area. It describes the surface shape and surface texture of the manufactured activated charcoal doped chitosan (AC-CS). Agglomerates of tiny fibres in various sizes and shapes, as well as a distinct binding crystalline structure, are how it expresses itself (Gong *et al.*, 2012). Additional particles are scattered into their outermost layer and some of the activated charcoal is embedded in the chitosan matrix's structure (Mohammed *et al.*, 2020).

According to the particle size distribution and XRD measurements, the average particle size of nanocomposite powder is 50nm. According to Bhuvaneswari *et al.*'s examination of the activated charcoal doped chitosan (AC-CS) by EDX, C, O, Na, Si, Cl, Ca & Fe were present (Bhuvaneswari *et al.*, 2022) as shown in Fig. 3. Because of this, it is suggested by the strong and clumped together narrow diffraction peaks of activated charcoal doped chitosan (AC-CS) indicating the resulting particles are crystalline in nature (Saranya Sukumar *et al.*, 2020).

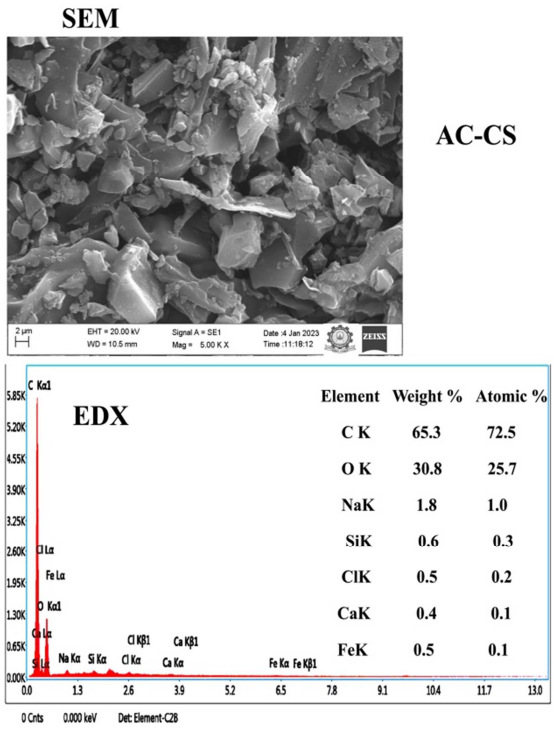


**Fig. 3.** The SEM-EDX graph of Activated Charcoal doped chitosan (AC-CS).

*UV-Visible Spectrophotometer*

Fig 4 displays the optical characteristics of biopolymer compounds after UV-visible spectroscopy analysis. According to Budnyak *et al.* (2016), Fig. 4 depicted UV absorption bands of activated charcoal doped chitosan (AC-CS) with maximum wavelengths at 308nm (Budnyak *et al.*, 2016). This suggests the emergence of activated charcoal doped chitosan (AC-CS) and its represents a typical Plasmon band.

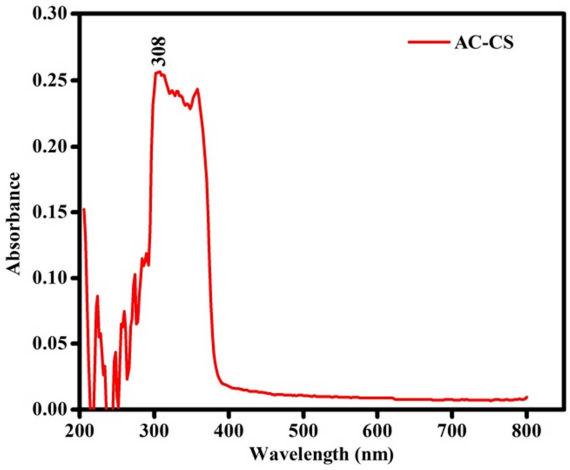


**Fig. 4.** The UV graph of Activated Charcoal doped chitosan (AC-CS).

The molecular weight of chitosan also affected the core of the absorption band, which controls both formation and stabilisation (Pritha Chakraborty *et al.*, 2018). Fig 4 demonstrated that the absorption bands following immobilisation, which showed the existence of activated charcoal doped chitosan (AC-CS), created the activated charcoal doped chitosan (AC-CS). This outcome demonstrates that activated charcoal doped chitosan (AC-CS) existed during the creation of the strong peak.

*Mechanism of photocatalytic catalytic degradation of the dye*

Malachite green dye deterioration is portrayed in Fig. 5 as a light-dependent process. A positive hole h+ is lifted inside the valence band during this process, and the dye is first adsorbed on the catalyst's surface (in this case, AC-CS). Next, the dye is subjected to ultraviolet light to excite valence electrons and allow them to migrate from the valence band to the conduction band. On the surface of the photocatalyst, adsorbed water molecules react with positive holes and free electrons to produce OH radicals, while free electrons change dissolved oxygen into superoxide anion O2 radicals. The dye molecules are broken down into less complex molecules like CO2 and H2O by these light-generated radicals (Ajmal *et al.*, 2014).

$$\text{AC-CS} + h\nu \rightarrow e^- + h^+ \quad (1)$$

$$H_2O + h^+ \rightarrow OH^{\cdot} + H^+ \quad (2)$$

$$O_2 + e^- \rightarrow O_2^{\cdot -} \quad (3)$$

$$OH + \text{MG dye} \rightarrow \text{degradable product} \quad (4)$$

$$O_2^- + \text{dye} \rightarrow \text{degradable product} \quad (5)$$

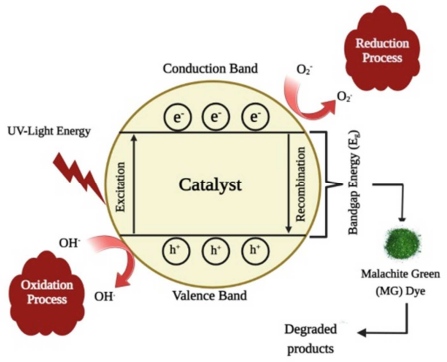


**Fig. 5.** Reaction mechanisms for the degradation of Malachite Green (MG).

*Photocatalytic Activity*

In order to determine the viability of enhancing the catalytic performance, the activated charcoal doped chitosan (AC-CS) components will first be evaluated individually before being evaluated collectively. The photodegradation effectiveness with various activated charcoal doped chitosan (AC-CS) illumination times throughout 160 min. is shown in Fig. 5(a, b). During UV light radiation treatment, the activated charcoal doped chitosan (AC-CS) displayed greater photocatalytic capacity. The increased degree of the interphase contact that can be obtained at activated charcoal doped chitosan (AC-CS) is thought to be the factor responsible for this particular occurrence (Dai *et al.*, 2013). Results demonstrated that raising the amount of activated charcoal doped chitosan (AC-CS) initially boosted the rate of photodegradation of Malachite Green, however beyond a certain point, it dropped and the photocatalyst's surface area that was exposed also arose. As shown in Fig. 6(a,b), the activated charcoal doped chitosan (AC-CS) reached the upper limit of the saturation point, and raising the amount afterwards resulted in reduced degradation of the dye.

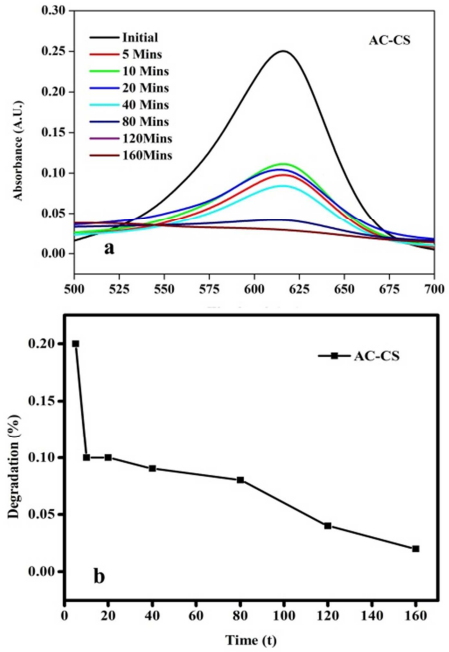


**Fig. 6.** The Photocatalytic graph of Activated Charcoal doped Chitosan (AC-CS) (a) represent Activated Charcoal doped Chitosan (AC-CS) (b) represent the degradation of dye from Activated Charcoal doped Chitosan (AC-CS).

**Conclusion**

Activated charcoal doped chitosan (AC-CS) was prepared using an enhanced technique and the material activated charcoal doped chitosan (AC-CS) has an FTIR spectrum that is consistent with the primary findings reported in the literature. The photocatalytic activated charcoal doped chitosan (AC-CS) was employed for conservational clean-up in the degradation of the dyes in the presence of UV irradiation. Activated charcoal doped chitosan (AC-CS) is highly stable during numerous applications. The dangerous aquatic contaminants, including malachite green dye were successfully broken down. Following continuous UV exposure, the photocatalytic reactions take place on the surface of the contaminants. Worldwide research on activated charcoal doped chitosan (AC-CS) for conservation cleaning in dye degradation has increased as a consequence of development.

**References**

**Abdel HA, Saad AM, Azzam ST, El-Wakeel BB, Mostafa MB.** 2018. Removal of toxic metal ions from wastewater using ZnO@Chitosan cores hell nanocomposite. Environmental Nanotechnology, Monitoring & Management. l **9,** 67-75.

**Afzal MZ, Sun XF, Liu J.** 2018. Enhancement of ciprofloxacin sorption on chitosan/biochar hydrogel beads. Sci Total Environ **639,** 560-569.

**Ajmal A, Majeed I, Malik RN, Idriss H, Nadeem MA.** 2014. Principles and mechanisms of photocatalytic dye degradation on $TiO_2$based photocatalysts: a comparative overview. RSC Adv **4(70),** 37003-37026.

**Annu A, Raja AN.** 2020. Recent development in chitosan-based electrochemical sensors and its sensing application, Int. J. Biol. Macromol **164,** 4231-4244,

**Aragunde H, Biarnés X, Planas A.** 2018. Substrate recognition and specificity of chitin deacetylases and related family 4 carbohydrate esterases. Int J Mol Sci **19,** 412

**Bhadra P, Mitra MK, Das GC, Dey R, Mukherjee S.** 2011. Interaction of chitosan capped ZnO nanorods with *Escherichia coli*," Materials Science and Engineering C. **31(5),** 929-937.

**Bhattacharyya S, Wang H, Ducheyne P.** 2012. Polymer-coated mesoporous silica nanoparticles for the controlled release of macromolecules. Acta Biomater **8(9),** 3429-3435.

**Bhuvaneswari P, Shanmugavadivu T, Sabeena G, Annadurai G, Sindhuja E.** 2022. Synthesis and Characterization of Chitosan with Silica (CS) Nanocomposite with Enhanced Antibacterial Activity. Int. J. Res. Pharm. Sci **13(1),** 1-8

**Budnyak TM, Yanovska ES, Kołodyńska D, Sternik D, Pylypchuk IV, Ischenko MV, Tertykh VA.** 2016. Preparation and properties of organomineral adsorbent obtained by sol-gel technology. Journal of Thermal Analysis and Calorimetry **125(3),** 1335-1351.

**Costa EM, Silva S, Pina C, Tavaria FK, Pintado MM.** 2012. Evaluation and insights into chitosan antimicrobial activity against anaerobic oral pathogens. Anaerobe **18(3),** 305-309.

**Dai K, Zhang X, Fan K.** 2013. Hydrothermal synthesis of single-walled carbon nanotube-TiO2 hybrid and its photocatalytic activity. Appl Surf Sci **270,** 238-244

**Fu YN, Li Y, Li G, Yang L, Yuan Q, Tao L, Wang X.** 2017. Adaptive chitosan hollow microspheres as efficient drug carrier. Biomacromolecules **18(7),** 2195-2204.

**Gong J, Wang X, Shao X, Yuan S, Yang C, Hu X.** 2012. Adsorption of heavy metal ions by hierarchically structured magnetite-carbonaceous spheres. Talanta **101,** 45-52.

**Hasmath Farzana M, Meenakshi S.** 2015. Visible light-driven photoactivity of zinc oxide impregnated chitosanbeads for the detoxification of textile dyes. Applied Catalysis A: General **503,** 124-134.

**Hassan M, Abou-Zeid R, Hassan E.** 2017. Membranes based on cellulose nanofibers and activated carbon for removal of Escherichia coli bacteria from water. Polymers (Basel) **9(8),** 335.

**He Q, Shi J.** 2011. Mesoporous silica nanoparticle based nano drug delivery systems: synthesis, controlled drug release and delivery, pharmacokinetics and biocompatibility. Journal of Materials Chemistry **21(16),** 5845.

**Huang Z, Li Z, Zheng L.** 2017. Interaction mechanism of uranium (VI) with three-dimensional graphene oxide-chitosan composite: Insights from batch experiments, IR, XPS, and EXAFS spectroscopy. Chemical Engineering Journal **328,** 066-1074.

**Jung KW, Choi BH, Hwang MJ.** 2016a. Fabrication of granular activated carbons derived from spent coffee grounds by entrapment in calcium alginate beads for adsorption of acid orange 7 and methylene blue. Bioresour Technol **219,** 185-195.

**Jung KW, Jeong TU, Kang HJ, Ahn KH.** 2016b. Characteristics of biochar derived from marine macroalgae and fabrication of granular biochar by entrapment in calcium-alginate beads for phosphate removal from aqueous solution. Bioresour Technol **211,** 108-116.

**Jurkic LM, Cepanec I, Pavelic SK, Pavelic K.** 2013. Biological and therapeutic effects of ortho-silicic acid and some ortho-silicic acid-releasing compounds: New perspectives for therapy. Nutrition & Metabolism **10(1),** 2.

**Li LH, Deng JC, Deng HR, Liu ZL, Xin L.** 2010. Synthesis and characterization of chitosan/ZnO nanoparticle composite membranes. Carbohydrate Research **345(8),** 994-998.

**Lijun You CI, Huang LU, Feifei AO, Wang Xiaocui Liu, Zhang Q.** 2018. Facile synthesis of high performance porous magnetic chitosan-polyethylenimine polymer composite for Congo red removal, International Journal of Biological Macromolecules **107,** 1620-1628.

**Liu X. Tian J, Li Y.** 2019. Enhanced dyes adsorption from wastewater via $Fe_3O_4$ nanoparticles functionalized activated carbon, Journal of Hazardous Materials **373,** 397-407.

**Maldiney T, Kaikkonen MU, Seguin J, Quentin Bessodes M, Airenne KJ, Seppo Yla, Scherman D, Richard C.** 2012. *In vitro* Targeting of Avidin-Expressing Glioma Cells with Biotinylated Persistent Luminescence Nanoparticles **23(3),** 472-478.

**Manzoor K, Ahmad M, Ahmad S, Ikram S.** 2019. Chapter 2-resorbable biomaterials: role of chitosan as a graft in bone tissue engineering, in: Materials for Biomedical Engineering, Elsevier, Amsterdam, Netherlands 23-44.

**Martins AF, Facchi SP, Follmann HD, Pereira AG, Rubira AF, Muniz EC.** 2014. Antimicrobial activity of chitosan derivatives containing N-quaternized moieties in its backbone: a review. Int. J. Mol. Sci **15(11),** 20800-20832.

**Mohammed MI, Ismael MK, Gonen M.** 2020. Synthesis of Chitosan-Silica Nanocomposite for Removal of Methyl Orange from Water: Composite Characterization and Adsorption Performance. IOP Conference Series: Materials Science and Engi- neering 745.

**Nguyen NT, Nguyen NT, Nguyen VA.** 2020. In Situ Synthesis and Characterization of ZnO/Chitosan Nanocomposite as an Adsorbent for Removal of Congo Red from Aqueous Solution. Advances in Polymer Technology **19-20,** 1-8.

**Onishi H, Nagai T, Machida Y.** 2020. Applications of chitin, chitosan, and their derivatives to drug carriers for microparticulated or conjugated drug delivery systems, in: Applications of Chitin and chitosan, CRC Press, Boca Raton, Florida, USA 205-231.

**Owda ME, Elfeky AS, Abou-Zeid RE, Saleh AI, Awad MA, Abdellatif H, Ahmed F, Elzaref AS.** 2022. Enhancement of Photocatalytic And Biological Activities of Chitosan/Activated Carbon Incorporated With $TiO_2$ Nanoparticles. Environmental Science and Pollution Research **29,** 18189-18201.

**Pouretedal HR, Keshavarz MH, Yosefi MH. Shokrollahi A, Zali A.** 2009. Photodegradation of HMX and RDX in the presence of nanocatalyst of zinc sulfide doped with copper. Iran. J. Chem. Chem. Eng **28,** 13-19.

**Pritha Chakraborty, Vakas Mustafa, Jayanthi Abraham.** 2018. Synthesis and Characterization of Chitosan Nanoparticles and Their Application in Removal of Wastewater Contaminants. Nature Environment and Pollution Technology **17(2),** 469-478 2018

**Sajid M, Ilyas M, Basheer C, Tariq M, Daud M, Baig N, Shehzad F.** 2014. Impact of nanoparticles on human and environment: review of toxicity factors, exposures, control strategies, and future prospects. Environ Sci Pollut Res Int **22(6),** 4122-43.

**Salari M, Sowti Khiabani M, Rezaei Mokarram R, Ghanbarzadeh B, Samadi Kafil H.** 2018. Development and evaluation of chitosan based active nanocomposite films containing bacterial cellulose nanocrystals and silver nanoparticles. Food Hydrocoll **84,** 414-423.

**Samadian H, Maleki H, Allahyari Z, Jaymand M.** 2020. Natural polymers-based lightinduced hydrogels: promising biomaterials for biomedical applications. Coord. Chem. Rev **420,** 213232.

**Saranya Sukumar, Agneeswaran Rudrasenan, Deepa Padmanabhan Nambiar.** 2020. Green-Synthesized Rice-Shaped Copper Oxide Nanoparticles Using *Caesalpinia bonducella* Seed Extract and Their Applications. ACS Omega **5,** 1040−1051.

**Sharififard H, Rezvanpanah E, Rad SH.** 2018. A novel natural chitosan/activated carbon/iron bionanocomposite: Sonochemical synthesis, characterization, and application for cadmium removal in batch and continuous adsorption process. Bioresour Technol **270,** 562-569.

**Sharma S, Ameta R, Malkani RK, Ameta SC.** 2013. Photocatalytic degradation of rose Bengal by semiconducting zinc sulphide used as a photocatalyst. J. Serbian Chem Soc **78,** 897-905.

**Sumayya AS, Muraleedhara Kurup G.** 2017. Marine macromolecules cross-linked hydrogel scaffolds as physiochemically and biologically favorable entities for tissue engineering applications. J. Biomater. Sci. Polym. Ed **28 (9),** 807-825.

**Sun J, Jiang H, Wu H, Tong C, Pang J, Wu C.** 2020. Multifunctional bionanocomposite films based on konjac glucomannan/chitosan with nano-ZnO and mulberry anthocyanin extract for active food packaging. Food Hydrocoll **107,** 105942.

**Tan G, Kaya M, Tevlek A, Sargin I, Baran T.** 2018. Antitumor activity of chitosan from mayfly with comparison to commercially available low, medium and high molecular weight chitosans, In Vitro Cell. Dev. Biol. Anim **54(5),** 366-374.

**Tang F, Li L, Chen D.** 2012. Mesoporous silica nanoparticles: synthesis, biocompatibility and drug delivery. Adv Mater **24(12),** 1504-34.

**Ullah R, Dutta J.** 2008. Photocatalytic degradation of organic dyes with manganesedoped ZnO nanoparticles. J. Hazard. Mater **156,** 194-200.

**Vichare R, Garner I, Paulson RJ, Tzekov R, Sahiner N, Panguluri SK.** 2020. Biofabrication of chitosan-based nanomedicines and its potential use for translational ophthalmic applications. Appl. Sci **10(12),** 4189.

**Wang H, Gong X, Miao Y.** 2019. Preparation and characterization of multilayer films composed of chitosan, sodium alginate and carboxymethyl chitosan-ZnO nanoparticles. Food Chemistry **283,** 397-403.

**Zabihi E, Babaei A, Shahrampour D, Arab-Bafrani Z, Mirshahidi KS, Majidi HJ.** 2019. Facile and rapid in-situ synthesis of chitosan-ZnO nano-hybrids applicable in medical purposes; a novel combination of biomineralization, ultrasound, and bio-safe morphology-conducting agent, International Journal of Biological Macromolecules **131,** 107-116.